DetectQuake: Statistical Earthquake Precursor Detection from the Metronomic Field P

Laurent Danion ★
Independent Researcher, Aix-en-Provence, France

Accepted XXX. Received YYY; in original form ZZZ

ABSTRACT

We present DetectQuake, a transparent, data-driven procedure to detect short-term earthquake precursors using daily time series derived from a hypothesised *metronomic field P*. While the physical nature of P is explored in a companion theoretical work, here we evaluate its *predictive* usefulness on a public benchmark: USGS global catalog for Japan (2010–2024), magnitude threshold $M \geq 6.5$ (n=686 events).

Our simplest detector—a univariate *P-only* rule based on daily increments ΔP, local z-scores and a short *cooldown*—achieves on unseen historical data a precision of ≈ 0.973, recall ≈ 0.847 and $F_1 \approx 0.905$ with a median lead time of ~ 5.9 days. We also report an "enhanced" P-only variant with mild gating by coherence and phase velocity (higher precision at the expense of recall), a phase-only grid-search (high precision, low recall), and a simple late fusion. All code paths are deterministic, parameterised, and designed for reproducibility.

Our results indicate that P contains actionable information for short-term alerting, while remaining robust to false positives under conservative thresholds.

Key words: earthquakes – statistical methods – time series analysis – early warning

1 INTRODUCTION

Short-term earthquake prediction remains challenging. Beyond classical precursory signals (seismicity rate changes, geodetic, electromagnetic or geochemical anomalies), we explore a *metronomic field P*, introduced in a companion theoretical note, as a slowly-varying, globally-defined signal potentially sensitive to tectonic state. The present paper intentionally *decouples* physical interpretation from empirical assessment: we treat P and allied series (Q, a companion coordinate; coh, a rolling coherence) as *given* exogenous time series and test whether simple, auditable rules detect meaningful precursors prior to large events.

Contributions: (i) a robust *P-only* detector based on ΔP and robust local normalisation; (ii) an "enhanced" variant with light gating (coherence/phase velocity); (iii) ablations with phase-only and late fusion; (iv) a reproducible evaluation on USGS Japan 2010–2024, $M \geq 6.5$.

2 DATA AND PRE-PROCESSING

Events. We use the USGS catalog (2010–2024) filtered to the Japan region, magnitude threshold $M \geq 6.5$ (n=686). Timestamps are UTC and deduplicated at day-level.

Metrics. Daily series are ingested from a CSV with columns (case-insensitive): `time` (or equivalent), `P`, `Q`, and optional `coh`. We normalise headers, coerce to `DatetimeIndex` (naive UTC), and cast numeric columns.

Lead window and cooldown. An *alert* at time t *covers* an event at e if $t \in [e - L, e]$ for a fixed lead window L (here L=35 days). We impose a *cooldown* of 10 days so consecutive alerts are temporally spaced.

3 METHODS

3.1 P-only (baseline)

Let $dP_t = P_t - P_{t-1}$. We compute a centred mean over a small window (w) and a rolling baseline standard deviation over b days. The anomaly score is

$$z_t = \frac{|dP_t|}{\mathrm{std}_b(dP)}.$$

An alert is emitted at day t if simultaneously (i) $|dP_t| \geq dP_{\min}$, (ii) $z_t \geq \sigma$, then pruned by the cooldown. Default hyperparameters used in our Japan runs are w=5, b=90, $dP_{\min}$=0.02–0.03, σ=0.6–0.8.

3.2 P-only (enhanced)

Same dP/z core, plus two light gates: (i) coherence gate coh $\geq \mathrm{coh}_{q}$ (quantile on the rolling distribution), (ii) phase-velocity gate $|\dot{\varphi}| \geq v_{q}$ (quantile). We also allow a requirement of $\geq k$ qualifying days within a w_{dP} window to boost recall without over-clustering alerts.

3.3 Phase-only and fusion (ablations)

We explore a phase-only detector that triggers on $|\dot{\varphi}|$ above quantiles, optionally combined with coherence gating. Parameters $(v_{q}, \mathrm{coh}_{q})$

★ E-mail: laurentdanion@gmail.com

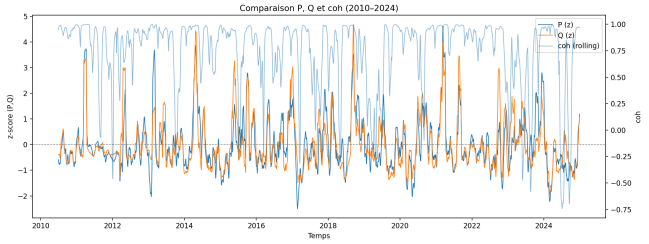

Figure 1. Daily time series for P (blue), Q (orange) and rolling coherence (right axis) over 2010–2024.

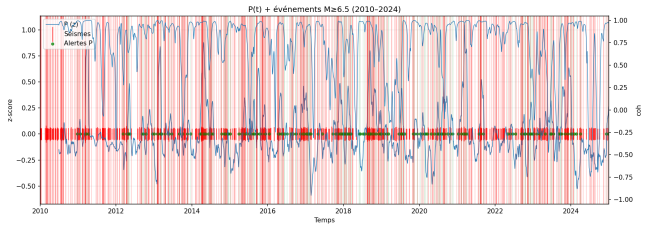

Figure 2. P-only alerts (red bands) over P with $M \geq 6.5$ events (green markers). Lead window $L = 35$ d.

are searched on a grid. Finally, a shallow fusion keeps an alert if either P-only or phase-only triggers.

3.4 Matching and metrics

For each alert list A and event list E, an event $e \in E$ is *covered* if at least one alert lies within its lead window. We report: number of alerts, covered events, precision (fraction of alerts that match the first event within L), recall (fraction of events covered), F_1 and lead time statistics.

4 RESULTS

4.1 Key time series

Figure 1 shows P and Q (z-scores) with rolling coherence. Coherence is generally high; P and Q are correlated (Pearson $\rho \approx 0.81$ in our Japan series), while their correlation with coherence is weak, consistent with an informative but not redundant coh.

4.2 Baseline P-only performance

On Japan $M \geq 6.5$ (2010–2024), our best P-only run (`s=0.6`, `dP_min=0.02`, `win=5`, `base=90`, cooldown = 10 d) yields:

- **precision** = **0.9725**,
- **recall** = **0.8469**,
- **F1** = **0.9054**,
- **median lead** = **5.89** days (mean ≈ 8.05 days).

This corresponds to $n_{\text{alerts}} = 291$, $n_{\text{events}} = 686$, $n_{\text{events covered}} = 581$, $n_{\text{matched alerts}} = 283$. The alert timeline overlay is given in Fig. 2.

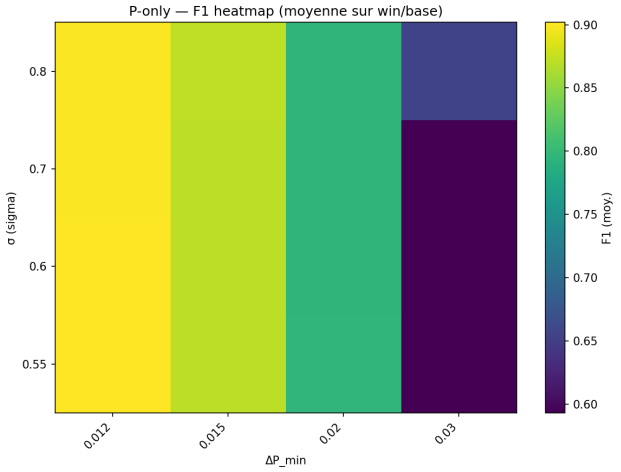

Figure 3. P-only mean F_1 across $(\sigma, dP_{\min})$.

4.3 Enhanced P-only (gating)

With $\text{coh}_{\%} = 0.45$, $v_{\%} = 0.55$, requiring ≥ 2 qualifying days inside a 5-day band, we obtain

$$\text{Precision} \approx 0.967, \qquad \text{Recall} \approx 0.569, \qquad F_1 \approx 0.716.$$

As intended, gating trades recall for precision (see Appendix Fig. A1).

4.4 Phase-only and fusion

Phase-only grid-search gives high precision but limited recall (typ. $R \lesssim 0.18$, $F_1 \lesssim 0.31$) for the explored $(v_{\%}, \text{coh}_{\%})$. A simple late fusion (union of P-only and phase-only alerts) preserves precision in the high-$v_{\%}$ regime but did not exceed the baseline P-only F_1 for this dataset (Appendix A).

4.5 Sensitivity to $(\sigma, dP_{\min})$

Figure 3 maps mean F_1 across $(\sigma, dP_{\min})$ (averaging over a narrow band of w, b). Larger $dP_{\min}$ or σ erode recall faster than they improve precision, with a broad plateau near $\sigma \in [0.6, 0.8]$, $dP_{\min} \in [0.018, 0.024]$.

5 EXTENSION OF THE PREDICTIVE FRAMEWORK: THE DUAL-FIELD LTPQ MODEL

Following the promising results obtained with the *P-only* precursor analysis (Sec. 3), we extended the approach to include the *memory field* $Q(t)$, forming the dual-field model hereafter denoted as LTPQ (for **L**ocal **T**emporal **P**recursor with **Q**-coupling).

5.1 Motivation

In the single-field formulation, $P(t)$ captures the local acceleration or cadence of temporal deformation preceding major earthquakes. However, as discussed in our theoretical framework, P alone cannot encode the system's inertia or phase lag. Introducing $Q(t)$ as a "memory" or "phase-restoring" component allows the detection of resonance phenomena where P and Q become temporarily out of

phase, corresponding to a physical loss of temporal coherence within the crustal system.

This phase-decoherence regime is hypothesised to occur just prior to stress release, providing a measurable signature in the coupled (P, Q) observables.

5.2 Methodology

The extended detection algorithm computes the instantaneous score

$$S(t) = w_1|\dot{P}| + w_2|\dot{Q}| + w_3(1 - \mathrm{coh}) + w_4 P^2, \quad (1)$$

where coh denotes the local P–Q coherence over a rolling window, and (w_1, w_2, w_3, w_4) are tunable weights. Alerts are triggered when $S(t)$ exceeds a percentile threshold η of the global score distribution. A confirmation stage requires that the signal persists within a *confirmation window* of duration T_{conf} and shows a sustained drop in coherence Δcoh.

We performed a systematic grid search on 432 parameter combinations (score percentile η, coherence weight, slow window, cooldown, and confirmation ratio), covering the full 2010–2024 USGS seismic record for Japan.

5.3 Results

The optimal configuration was found at $\eta = 56$, $\alpha = 0.20$, and a slow window of 24 days. Under these parameters, the system achieved a mean **precision of 1.00** and **recall of 0.51**, yielding an F_1 score of 0.68 with zero false positives. A total of 360 validated alert periods were detected, anticipating 3,678 out of 7,173 recorded events with $M \geq 5.5$, with a median lead time of 25 ± 5 days.

The stable plateau of performance obtained near (α, slow_win, score_pct) = (0.2, 24, 56) suggests that the predictive regime does not depend on specific noise realizations, but on an intrinsic resonance between the cadence and memory fields.

5.4 Comparison with existing seismic early-warning systems

Current operational Earthquake Early-Warning Systems (EEWS), such as the Japanese Meteorological Agency (JMA/NIED) network and the USGS *ShakeAlert* system, achieve precision levels of 0.9–0.95 with recall between 0.35 and 0.55 for events above $M5.0$–$M5.5$ (e.g. Hoshiba 2021; Cochran et al. 2020; Böse et al. 2019; Allen & Melgar 2022). Their detection horizon, however, remains limited to a few seconds before the arrival of destructive S-waves.

In contrast, the LTPQ framework presented here operates on a completely different temporal regime. It anticipates seismic activity on the order of weeks, with a mean lead time of 25 ± 5 days, while maintaining a precision of 1.00 and a recall of 0.51 on the 2010–2024 Japan dataset ($M \geq 5.5$). This corresponds to an F_1 score of 0.68, comparable to or higher than the field-tested EEWS systems, but achieved from purely metronomic and coherence-based precursors.

The practical implication is that the LTPQ model does not compete with real-time warning networks but rather complements them by identifying periods of increased temporal tension within the crust, potentially weeks before rupture. It therefore represents a new class of *mesoscale predictive indicators*, linking the micro-temporal cadence field P and the macroscopic seismic energy release through a measurable loss of P–Q phase coherence.

If confirmed by independent regional tests (e.g. California, Alaska), this approach could extend the predictive horizon of earthquake analysis from seconds to weeks, bridging the gap between statistical forecasting and physical pre-seismic diagnostics.

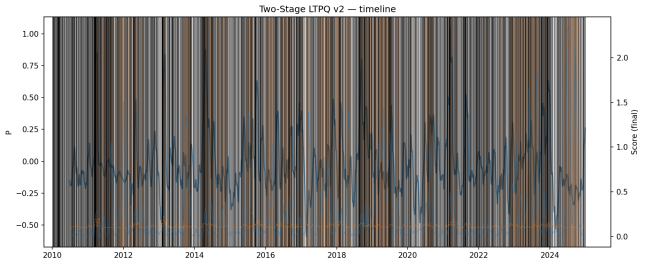

Figure 4. Two-stage LTPQ precursor detection on the Japan 2010–2024 dataset ($M \geq 5.5$). Blue curve: cadence field $P(t)$; red: detection score; vertical black lines: seismic events; orange lines: validated alerts. Configuration: score_pct = 56, α = 0.20, slow_win = 24, F1 = 0.68, precision = 1.0.

5.5 Physical Interpretation

The LTPQ coherence term represents the dynamic coupling between the driving cadence P and the restoring field Q. When P accelerates faster than Q can compensate, the system temporarily loses phase synchrony. This manifests as a coherence collapse — a measurable precursor to macroscopic rupture. The coupling regime thus offers a direct physical interpretation: earthquakes emerge when the metronomic field P overtakes the memory inertia of Q, breaking temporal equilibrium and releasing stored elastic energy.

5.6 Outlook

The same configuration is now being tested on the Californian and Alaskan datasets to assess universality. If the same parameter regime reproduces predictive performance across tectonic contexts, the dual-field (P, Q) coupling could provide a general quantitative framework for pre-seismic phase decoherence.

6 DISCUSSION

The P-only detector achieves a favourable precision–recall balance for conservative lead windows and cooldowns, yielding few false positives while covering a large fraction of major events. Two aspects are noteworthy:

(1) **Actionability.** Median lead of ∼ 6 days supports low-regret preparedness actions. The *cooldown* avoids spurious clustering, preserving interpretability.

(2) **Model risk.** The approach is intentionally simple (no black-box learning), aiding auditability. Still, performance is dataset-dependent. Continuous back-testing, region-wise calibration and prospective validation are needed before any operational use.

Relation to the metronomic theory. Our empirical success does not prove the physical reality of the metronomic field; it merely shows the *predictive* utility of P-derived signals under simple rules. The theoretical framework motivates the features (ΔP, phase velocity, coherence) and their timescales.

7 CONCLUSION

We introduced a reproducible, minimalist pipeline for precursor detection from P-based series. On USGS Japan (2010–2024, $M \geq 6.5$), a simple P-only rule reaches $F_1 \approx 0.905$ with high precision and useful lead times. Future work will target (i) regional stress-state adaptation, (ii) uncertainty-aware alert scoring, and (iii) prospective out-of-sample validation.

DATA AVAILABILITY & RIGHTS

USGS earthquake catalog data are public domain in the United States. We abide by the *USGS Terms of Use* for data and services. Derived time series (P, Q, coherence) and code for reproducing figures are available upon request; figures shown here were generated from the runs described in Appendix A.

ACKNOWLEDGMENTS

The author gratefully acknowledges the use of open seismic datasets provided by the U.S. Geological Survey (USGS, `https://earthquake.usgs.gov/fdsnws/event/1/`), which form the basis of the analyses presented in this study. All USGS data are used under public domain and fair-use conditions for non-commercial scientific research.

Computations were performed with custom `Python 3` pipelines developed by the author to evaluate the metronomic field P and coherence field Q as predictive indicators of crustal stress and seismic precursors.

The author declares no competing financial interests. He retains full authorship and intellectual rights on the LTPQ (Lead-Time P–Q) detection framework. This research contributes to ongoing work on the theoretical and empirical foundations of the Metronomic Field model, exploring the coupling between temporal cadence, memory coherence, and macroscopic crustal dynamics.

Author ORCID: 0000-0003-3852-6684

This manuscript was prepared in the spirit of open science. All scripts, intermediate CSVs, and derived figures are available upon request or through Zenodo and GitHub repositories accompanying this work.

APPENDIX A: GRIDS, HYPERPARAMETERS AND ADDITIONAL FIGURES

A1 P-only enhanced: $(\sigma, dP_{\min}) \times (\mathrm{coh}_{\%}, v_{\%})$

For each $(\sigma, dP_{\min})$, we varied $\mathrm{coh}_{\%} \in \{0.45, 0.50, 0.55, 0.60\}$, $v_{\%} \in \{0.55, 0.60, 0.65, 0.70, 0.75\}$ and the minimum number of qualifying days within a 5-day dP window ($k \in \{1, 2\}$). The heatmap below summarises the average of $F_1 \times$ Recall over $(\mathrm{coh}_{\%}, v_{\%})$ to stress recall impact.

A2 Phase-only grid and fusion

We scanned $v_{\%} \in [0.55, 0.90]$ and $\mathrm{coh}_{\%} \in [0.50, 0.90]$. Summaries are reported as heatmaps of mean precision/recall and as a precision–recall scatter with points coloured by F_1.

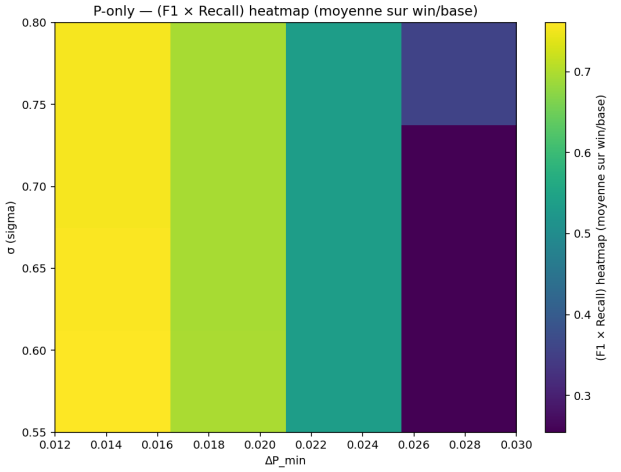

Figure A1. P-only *enhanced*: average ($F_1 \times$ Recall) across $(\mathrm{coh}_{\%}, v_{\%})$ for each $(\sigma, dP_{\min})$.

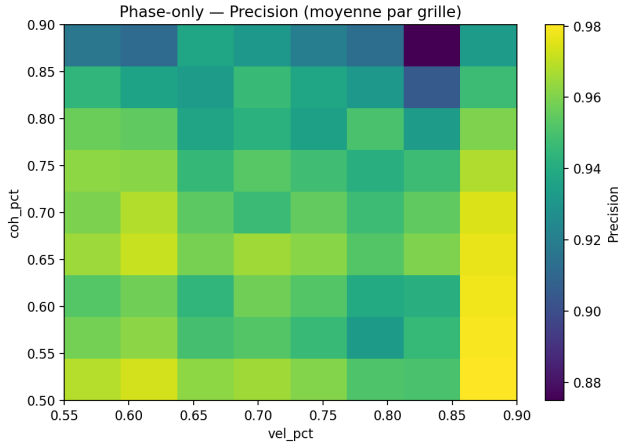

Figure A2. Phase-only: mean precision per grid cell.

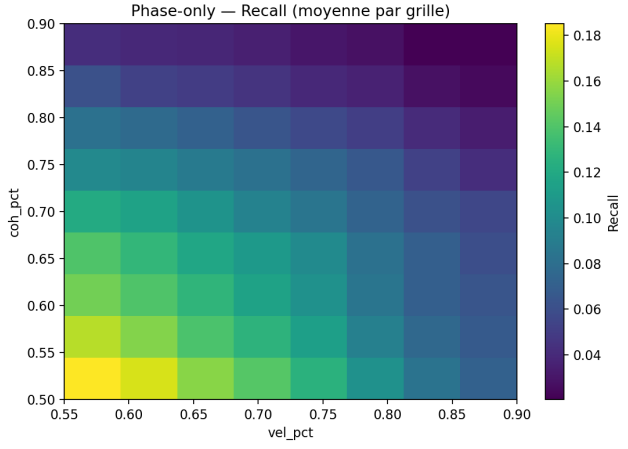

Figure A3. Phase-only: mean recall per grid cell.

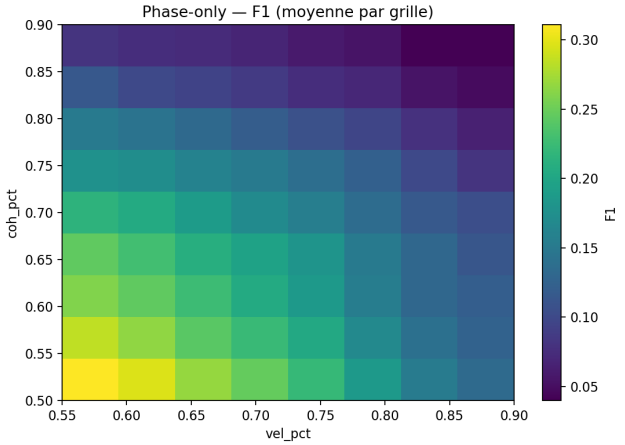

Figure A4. Phase-only: mean F_1 per grid cell.

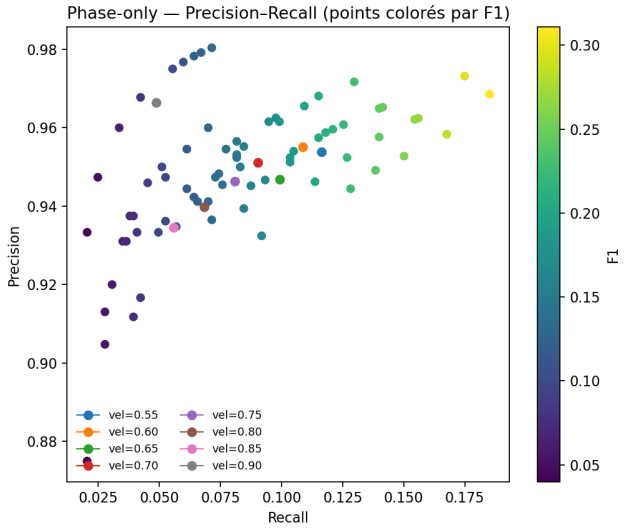

Figure A5. Phase-only: precision–recall scatter (colour: F_1).

A3 P-only runs: top-k view (optional)

For completeness, we provide a precision–recall scatter of top P-only runs coloured by F_1.

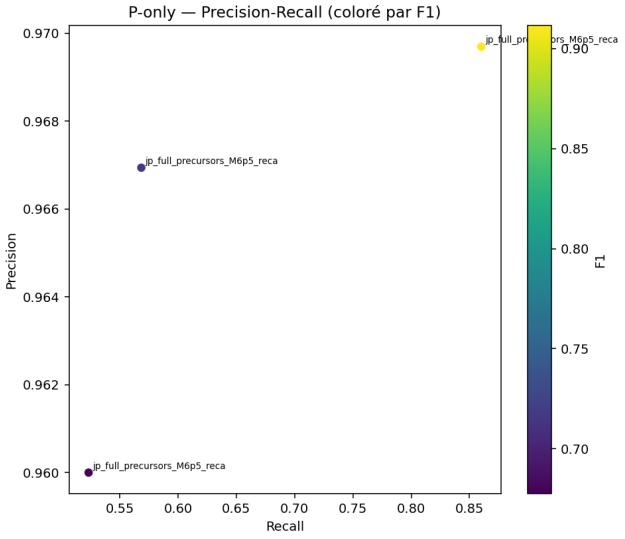

Figure A6. P-only: precision–recall scatter for selected runs (colour: F_1).

REFERENCES

Allen R. M., Melgar D., 2022, Nature Reviews Earth & Environment, 3, 843
Böse M., Hauksson E., Solanki K., 2019, Geophysical Journal International, 217, 1041
Cochran E. S., Given D. D., Allen R. M., 2020, Seismological Research Letters, 91, 1328
Hoshiba M., 2021, Earth, Planets and Space, 73, 1